

LENSING MEASUREMENTS OF SZ-DISCOVERED CLUSTERS IN THE SOUTHERN COSMOLOGY SURVEY

RACHEL N. MCINNES^{1*}, FELIPE MENANTEAU², ALAN F. HEAVENS¹, JOHN P. HUGHES², RAUL JIMENEZ³, RICHARD MASSEY¹, PATRICK SIMON¹, & ANDY N. TAYLOR¹

ABSTRACT

We present the first lensing mass measurements of Sunyaev-Zel'dovich (SZ) selected clusters. Using optical imaging from the Southern Cosmology Survey (SCS), we present weak lensing masses for three clusters selected by their SZ emission in the South Pole Telescope survey (SPT). Curiously, we find one additional 2.5σ peak in the lensing maps which seems to coincide with a low significance peak in the published SZ maps. We also study 38 optically-selected clusters in $\simeq 8$ square degrees of the SCS survey. We fit Navarro, Frenk and White (NFW) profiles, and find that the SZ clusters have amongst the largest masses, as high as $5 \times 10^{14} M_{\odot}$. Using the best fit masses for all the clusters, we analytically calculate the expected SZ integrated Y parameter for comparison with the SPT observations.

Subject headings: gravitational lensing — cosmology: observations — galaxies: clusters: general

1. INTRODUCTION

Galaxy clusters are the largest gravitationally bound objects in the Universe and can be used as cosmological probes because their formation and evolution rate are sensitive to different cosmological parameters (e.g., Evrard 1989; Haiman et al. 2001; Allen et al. 2004). In order to use galaxy clusters as cosmological probes, it is necessary to know the number of clusters as a function of mass and redshift, $N(m, z)$. The abundance of galaxy clusters at high redshift is particularly sensitive to different cosmological models. To probe cosmology and dark energy we must observe galaxy clusters at high redshift, z , and obtain mass estimates for them.

Observations of the Sunyaev-Zel'dovich (SZ) effect (Sunyaev & Zel'dovich 1981) are a powerful way to probe galaxy clusters by detecting the hot cluster gas (Birkinshaw 1998). SZ-detected clusters are in principle particularly powerful as they can be seen to high redshifts. The intensity of the SZ effect summed over the entire cluster closely tracks the mass of the cluster (Motl et al. 2005). X-ray or SZ effect mass estimates are based on simplified assumptions such as a hydrostatic equilibrium for the cluster gas. It is becoming increasingly apparent, however, that we cannot fully model the complex gas physics in clusters within a simple framework. Nonetheless, it will be very challenging to calibrate cluster masses at high redshift, so in order to use SZ observations to probe cluster properties and cosmological models it is important to understand the relationship between mass and SZ observables in lower redshift systems. Gravitational lensing facilitates the calibration of the SZ observables to obtain accurate masses for SZ detections (Lewis & King 2006; Sealfon et al. 2006). A large area in the southern sky is currently being surveyed in SZ by the Atacama Cosmology Telescope (ACT) and the South Pole Telescope (SPT).

Gravitational lensing is dependent only on the projected mass distribution of the lens and so it is possible to study the mass distribution independent of its form, including the distribution of dark matter. Gravitational lensing causes small (\sim a few %) changes to the shape of individual galaxies. The net distortion averaged over an area of sky can be measured to give us statistical properties of the matter distribution between us and the lensed source. By measuring the shapes and orientations of galaxies over a large area of sky, the average *shear* can be measured, which can be used to reconstruct the mass distribution in the region (Kaiser & Squires 1993); for a review see Munshi et al. (2008).

In this paper we present measurements of weak lensing masses for clusters which were, for the first time, detected blind by their SZ decrement (Staniszewski et al. 2008). We also include mass measurements from 25 optically-detected clusters.

This paper is structured as follows: in §2 we present the data and discuss the image processing; §3 describes the gravitational lensing methods used; the mass measurements are presented in §4 and we compare with measurements from other techniques and calculate the Y parameters. Throughout this paper we assume a flat cosmology with $\Omega_m = 0.27$, $\Omega_{\Lambda} = 0.73$ and $H_0 = 100h$ km s⁻¹Mpc⁻¹ with $h = 0.71$.

2. OBSERVATIONS

We use publicly-available data from the Blanco Cosmology Survey. This is a National Optical Astronomy Observatory Large Survey Project observing 60 nights over 4 years on the Blanco 4m telescope at the Cerro Tololo InterAmerican Observatory in Chile. The Mosaic II camera is being used for a deep, four-band optical (*griz*) survey of two 50 deg² patches of the southern sky. Two areas of southern sky have been targeted, centered on 23^h00^m , $-55^{\circ}12^m$ and 05^h30^m , $-52^{\circ}47^m$. These fields lie within a larger area of the southern sky which ACT and SPT plan to survey. The paper is based on observations taken in 2005, except from 2 clusters from 2006 data. The seeing varies between $0.81''$ and $1.09''$ with a mean of $0.89''$.

The image reduction was carried out using the Rutgers Southern Cosmology Pipeline. This performs flat field

¹ Scottish Universities Physics Alliance (SUPA), Institute for Astronomy, University of Edinburgh, Blackford Hill, Edinburgh, EH9 3HJ, U.K.

² Rutgers University, Department of Physics & Astronomy, 136 Frelinghuysen Road, Piscataway, NJ 08854, USA

³ ICREA & ICE(CSIC)-IEEC, UAB campus, Bellaterra 08193, Spain

* rnm@roe.ac.uk

correction, CCD calibration, removal of saturated star bleed-trails, and generation of bad pixel masks. Next the images were aligned, stacked and median combined using SWarp (Bertin 2006); an astrometric solution was found by matching stars to sources in the US Naval Observatory Catalog. Additional image masks were made by hand, to remove large saturated stars, satellite trails and other blemishes in the image. Approximately 8% of the area was excluded by the masks. For more information on the image reduction pipeline see Menanteau et al. (2008). Note that we use AB magnitudes throughout.

To calculate photometric redshifts (photo- z s), multi-band SExtractor (Bertin & Arnouts 1996) g, r, i, z isophotal magnitudes were used to find redshift probability distributions of each object. This was done using the BPZ code (Benítez 2000). For more information on the photometric redshifts see Menanteau et al. (2008).

We focused on 4 clusters found in SZ (Staniszewski et al. 2008) and also 38 optical clusters selected from $\simeq 8$ square degrees (Menanteau et al. 2008). Of the 38 clusters, we found non-zero mass estimates for 25 clusters, and upper limits for the remaining clusters. We do not consider 5 of the clusters as they are in regions only observed in a single exposure.

3. WEAK LENSING ANALYSIS

We utilized the i band data, 3 co-added exposures of 450s each, for our shear analysis. We measured galaxy shapes using the Kaiser, Squires & Broadhurst (1995) (KSB) method. Several variants of KSB have been developed; our pipeline is based on that described in Bacon, Refregier & Ellis (2000) and labelled “MB” in Heymans et al. (2006), but has been automated to process rapidly the large SCS data set. We independently tested our method’s performance on simulated images containing a known shear signal, from the Shear TEsting Programme (STEP) (see Heymans et al. 2006; Massey et al. 2007). Our method underestimates shear, but consistently throughout a wide range of observing conditions, which is henceforth compensated for in our shear measurements by applying a calibration factor of $1/(0.82 \pm 0.05)$.

Our pipeline locates individual galaxies via the IMCAT⁵ HFINDPEAKS algorithm, measures their quadrupole shape moments using a Gaussian weight function of width $4r_g$, and fits their shear polarizability factor $\frac{1}{2}\text{Tr}(P^\gamma)$ as a function of galaxy size. We excluded galaxies smaller than 1.8 times the measured seeing, or with signal to noise ratio less than 5. This lead to a number density $n = 9$ galaxies per square arcminute, and a limiting magnitude of $i \sim 23$. This corresponds to a median photometric redshift of $z = 0.65$ (Coil et al. 2004); 69% of galaxies in our catalog also had photo- z s, and these measured values lead to a consistent redshift distribution (Menanteau et al. 2008)

Departing from the “MB” pipeline, we performed star/galaxy separation via the automated THELI algorithm (Erben et al. 2005). We also automated the removal of galaxies with abnormally large values of shear polarizability, smear polarizability or ellipticity, which was present in the “MB” method but labor intensive and slow.

The observed shapes of galaxies were finally corrected for the blurring effect of the Point Spread Function (PSF). We measured the PSF from the shapes of the 0.5 unsaturated stars per square arcminute between magnitudes 22.0 and 18.1 (signal-to-noise 55 to 1670). The PSF typically has an ellipticity of 0.035 ± 0.019 , where the error is the standard deviation throughout the survey. Optical effects and temporal variation of the atmosphere and telescope between dithered exposures produce complex patterns in PSF size and ellipticity within each field. This variation was fitted as a sum of polynomials (of order 4 in the x and y directions) plus sums of sines and cosines (of orders up to 4 in x and 8 in y).

In order to obtain mass estimates, the binned output from IMCAT’s ETPROFILE routine was used to carry out a χ^2 -fit of the reduced shear to the universal Navarro, Frenk & White (1996), NFW profile. The concentration index of the halo was taken as a function of mass and cluster redshift (Dolag et al. 2004) so we had a one-parameter system. Where possible, the cluster center for the NFW fit was taken to be the peak of the projected mass distribution, and in cases where we were unable to find a center from the mass distribution, the luminosity-weighted center was used. For a robust treatment of missing regions of data we use a Wiener-filtered mass reconstruction method (Hu & Keeton 2002, section II) to reconstruct the surface mass density. To address the mass-sheet degeneracy the average surface mass density is set to zero when averaged over the whole field of view (half a square degree). The Wiener-filtered maps were used solely to find the center of the cluster, then the NFW model was fitted to the data (not the Wiener reconstructed maps). Our Wiener-filtered reconstruction was done as follows: the two-point correlation function of the lensing convergence, used as prior for the Wiener reconstruction, was estimated from the shear-shear correlation (Bartelmann & Schneider 2001) $\xi_+(\theta)$ in the data itself. In order to have a smooth prior, we fitted the measured ξ_+ with $\xi_+(\theta) = a/(1 + b\theta)$ where a and b are constants determined by the fit. To obtain signal-to-noise maps of the lensing maps we divided the maps by the r.m.s.-variance between 200 noise realisations, which were generated by randomly rotating the ellipticities of the sources followed by a Wiener reconstruction. The signal-to-noise maps were then used to confirm the cluster centers found in the mass maps.

4. RESULTS

The Wiener-filtered mass reconstructions for three of the SPT SZ-detected clusters are shown in Figure 1. The fourth of the SZ clusters is at redshift $z \sim 0.88$ and we do not detect a significant lensing signal. Our mass maps of clusters SPT0517-5430, SPT0509-5342, and SPT0528-5300 have signal-to-noise ratios of 2, 2.5 and 1.5 respectively.

The mass reconstruction of SPT0528-5300, at $z \sim 0.7$, is shown in the lower panel of Fig. 1. There is a second peak in the mass, at a significance of 2.5 which is $6.5'$ from the brightest cluster galaxy (BCG). It is at $05^h27^m56.9^s - 53^h06^m06.5^s$ and we estimate it to be more massive, at $5.61_{-4.99}^{+7.84} \times 10^{14} M_\odot$. On examination of Staniszewski et al. (2008, Fig.1), a decrement in the SZ appears to be present, although more faintly than the SPT detection threshold. There is no statistically

⁵ [http://www.ifa.hawaii.edu/~sim\\$kaiser/imcat](http://www.ifa.hawaii.edu/~sim$kaiser/imcat)

significant difference between the redshift distribution of optically selected galaxies in a $3'$ radius around this location compared to the redshift distribution of the surrounding 0.4 square degree region. We suggest that this region is looked at further in X-ray, and with deeper optical data to further examine its properties.

Figure 2 displays the comparison between our lensing mass and the optical mass estimate. We see that the blind SZ detections are amongst the most massive of the clusters, with masses generally exceeding $10^{14} M_{\odot}$. We also see that there is some correlation between the masses determined using the optical luminosity (Menanteau et al. 2008; Menanteau & Hughes 2008), M_{L200} , of all the clusters and the weak lensing masses, giving some justification for using the optical luminosity as a mass proxy. Interestingly, the most discrepant of the SZ clusters has conflicting optical and X-ray mass estimates, suggesting that M_{L200} is overestimated.

We calculated the expected Compton y parameter and its integral over solid angle, $Y \equiv \int d\Omega y(\Omega)$ for the clusters, given the NFW profile and the concentration index c_s . We can obtain an analytic result that agrees, within 25%, with the empirical scaling relations of Motl et al. (2005) and Nagai (2006) if we assume that gas follows dark matter:

$$Y(M_{200}) = \frac{c_s \sigma_T \Omega_b (1+z) (GH_0)^{2/3} \delta_{200}^{1/3} M_{200}^{5/3}}{6m_e c^2 D_A^2 \alpha \Omega_m [\ln(1+c_s) - c_s/(1+c_s)]^2} \quad (1)$$

where z is the cluster redshift, D_A its angular diameter distance, M_{200} its mass within an overdensity $\delta_{200} = 200$, α is the total pressure divided by the electron pressure. Assuming ions and electrons are in thermal equilibrium with a Helium mass fraction of 0.24, $\alpha = 1.93$. We also assume the concentration index

$$c_s(M_{200}) = 9.59(1+z)^{-1} (M_{200}/10^{14} h^{-1} M_{\odot})^{-0.102} \quad (2)$$

(Dolag et al. 2004), but note that this is for a $\sigma_8 = 0.9$ cosmology, higher than current estimates (Komatsu et al. 2009). These were computed for all the clusters for which we have mass detections. With a uni-

form prior on masses, we record in Table 1 the most likely masses and asymmetric one-sigma errors for the SPT SZ clusters (first four rows) and also for the optically-detected clusters in the 23 hour field. Predicted Y and average y within r_{200} are also shown here, along with the R.A. and Dec. of the cluster centre used. These $\langle y \rangle$ values should be compared with those derived from the SZ observations. To the extent that we can estimate $\langle y \rangle$ from the published maps, our results seem to be about 50% higher than observed, but within the errors expected from the mass determinations.

5. CONCLUSIONS

We have measured, for the first time, weak lensing masses of clusters detected by their Sunyaev-Zel'dovich signature. Of the four clusters detected by the SPT and published recently by Staniszewski et al. (2008), we have detected three of them, using optical imaging data from the Southern Cosmology Survey. The fourth cluster, at redshift of 0.88, is too distant to detect with these optical data. We have also presented weak lensing mass estimates for other clusters detected optically in the SCS, and found that the published SZ clusters have masses at the upper end, $10^{14} - 10^{15} M_{\odot}$. We fitted NFW profiles to the clusters using the concentration index-mass relation of Dolag et al. (2004), and found good fits. Furthermore, we made predictions for the integrated Compton Y parameter for the clusters in the survey to be compared with SZ observations.

The authors thank Catherine Heymans for many useful discussions. RNM acknowledges the award of an STFC studentship. FM and JPH acknowledge financial support from the National Science Foundation under the PIRE program (award number OISE-0530095). RJM acknowledges financial support through FP7 grant MIRG-CT-208994 and STFC Advanced Fellowship PP/E006450/1. We acknowledge the support of the European DUEL Research Training Network (MRTN-CT-2006-036133).

REFERENCES

- Allen, S. W., Schmidt, R. W., Ebeling, H., Fabian, A. C. & van Speybroeck, L., 2004, MNRAS, 353, 457
- Bacon, D., Refregier, A. & Ellis, R., 2000, MNRAS, 318, 625
- Bartelmann, M. & Schneider, P., 2001, Phys. Rep., 340, 291
- Benítez, N., 2000, ApJ, 536, 571
- Bertin, E., Arnouts S., 1996, A&AS, 117, 393
- Bertin, E., 2006, SWARP RESAMPLE AND COADD SOFTWARE
- Birkinshaw, 1999, Phys. Rep., 310, 97
- Coil et al., 2004, ApJ, 617, 765
- Dolag K., Bartelmann M., Perrotta F., Baccigalupi C., Moscardini L., Meneghetti M. & Tormen G., 2004, A&A, 416, 853
- Erben, T. et al., 2005, Astronomische Nachrichten, 326, 432
- Evrard, A. E., 1989, ApJ, 341, L71
- Haiman, Z., Mohr, J. J. & Holder, G. P., 2001, ApJ, 553, 545
- Heymans, C. et al., 2006, MNRAS, 371, 750
- Hu, W. & Keeton, C. R., 2002, Phys. Rev. D, 66, 6
- Kaiser, N. & Squires, G. 1993, ApJ, 404, 441
- Kaiser, N., Squires, G. & Broadhurst, T., 1995, ApJ, 449, 460
- Komatsu, E. et al., 2009, ApJS, 180, 330
- Lewis, A. & King, L., 2006, Phys. Rev. D, 73, 063006
- Massey, R. et al., 2007, MNRAS, 376, 13
- Menanteau, F. et al., 2008, ApJ in press (arXiv:0808.0214)
- Menanteau, F. & Hughes, J. P., 2008, ApJ in press (arXiv:0811.3596)
- Motl, P. M., Hallman, E. J. & Burns, J. O., 2005, ApJ, 623, 63
- Munshi, D., Valageas, P., van Waerbeke, L., Heavens, A.F., 2008, Phys. Rev. 462, 67
- Nagai, D., 2006, ApJ, 650, 538
- Navarro, J. F., Frenk, C. S. & White, S. D. M., 1996, ApJ, 462, 563
- Sealfon, C., Verde, L. & Jimenez, R., 2006, ApJ, 649, 118
- Staniszewski, Z. et al., 2008, arXiv:0810.1578
- Sunyaev & Zel'dovich, 1981, Astrophysics and Space Physics Reviews, 1, 1

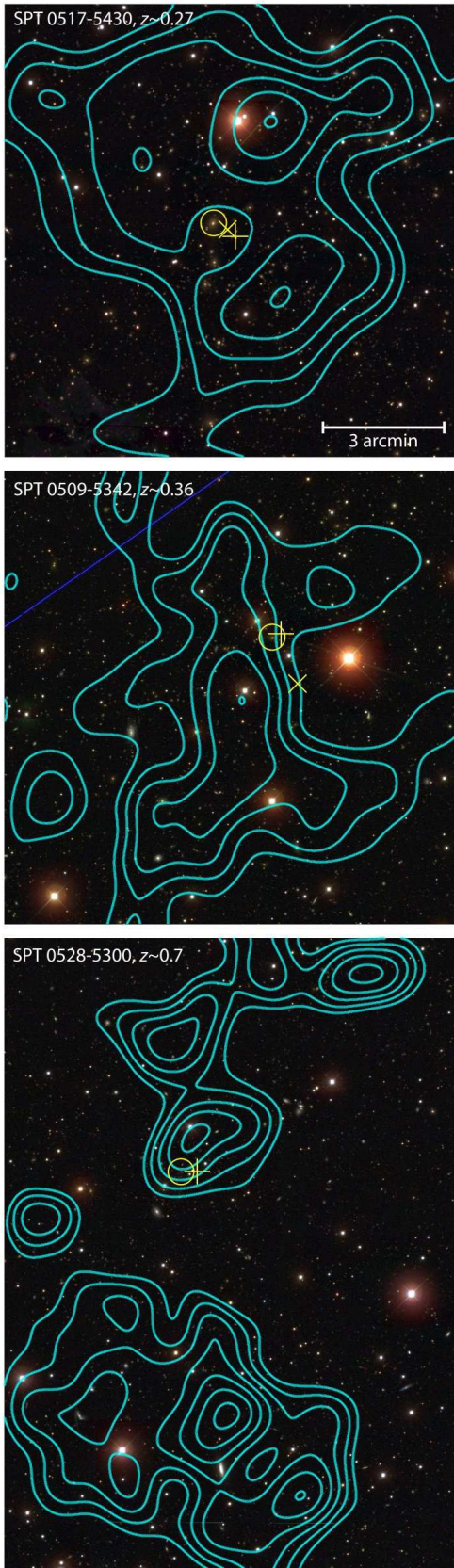


FIG. 1.— Lensing mass reconstructions for SZ-detected clusters. Contours show the projected lensing convergence (mass distribution), at 1%, 1.5%, 2%, ... 4%. A circle indicates the BCG in each optically selected cluster, an \times indicates a peak in X-ray emission, and a $+$ denotes the SZ peak.

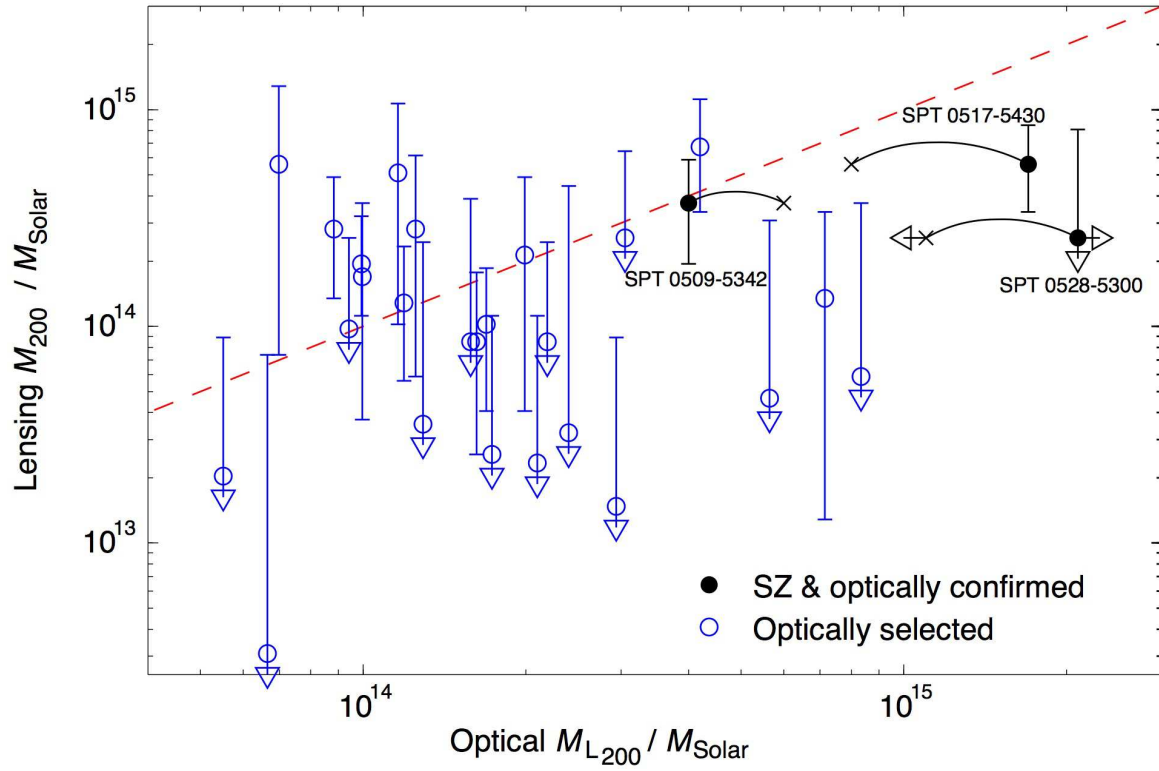


FIG. 2.— Lensing mass M_{200} measurement against optical mass M_{L200} for SZ and optically selected clusters. Filled circles show the SZ-selected and optically confirmed clusters, while empty circles denote clusters observed optically. Lower error bars marked with a triangle signify that the lower error reaches zero. X-ray mass estimates are shown as an \times on this plot for the 3 SZ-detected clusters, joined by an arc to the optical estimate. The dashed line is a one to one relationship between M_{L200} and the lensing M_{200} to guide the eye.

TABLE 1
CLUSTER WEAK LENSING, OPTICAL, X-RAY MASS ESTIMATES & PREDICTED SZ

ID	R.A. Center of NFW fit	Dec.	Center	z_{photo}	M_{L200} ($10^{14}M_{\odot}$)	M_{LX} ($10^{14}M_{\odot}$)	M_{200}^{Lens} ($10^{14}M_{\odot}$)	$\langle y \rangle$ (μK)	Y_{200} (10^{-5} arcmin^2)
SPT 0517-5430	05:16:27.3	-54:27:39.4	map	$0.27^{+0.02}_{-0.02}$	17	8	$5.61^{+2.88}_{-2.23}$	280.2	302.9
SPT 0509-5342	05:09:27.2	-53:45:18.2	map	$0.36^{+0.02}_{-0.02}$	4	6	$3.70^{+2.17}_{-1.76}$	228.8	110.5
SPT 0528-5300	05:28:02.2	-52:58:48.0	map	$0.70^{+0.03}_{-0.02}$	≥ 21	< 11	$2.56^{+5.54}_{-2.56}$	332.1	39.8
SPT 0547-5345	05:46:41.1	-53:44:52.1	lum.	$0.88^{+0.08}_{-0.04}$	≥ 4	10	< 2.56	-	-
SCSO J232540.2-544430.9	23:25:32.2	-54:44:21.5	lum.	0.10 ± 0.02	2.10	-	$0.23^{+0.89}_{-0.23}$	6.8	5.8
SCSO J232230.9-541608.3	23:22:27.2	-54:16:26.9	lum.	0.12 ± 0.02	1.62	-	$0.85^{+0.92}_{-0.59}$	26.9	38.9
SCSO J233000.4-5443707.7			n/a	0.14 ± 0.02	1.19	-	-	-	-
SCSO J232419.6-552548.9	23:24:23.6	-55:27:42.7	map	0.18 ± 0.04	1.19	-	$1.28^{+1.05}_{-0.72}$	48.3	41.9
SCSO J233106.9-555119.5	23:31:08.2	-55:50:56.4	lum.	0.19 ± 0.04	0.55	-	$0.20^{+0.69}_{-0.20}$	7.5	1.7
SCSO J233252.9-561454.1	23:32:51.4	-56:15:29.8	lum.	0.20 ± 0.03	1.17	-	< 0.09	-	-
SCSO J233215.5-544211.6	23:32:17.1	-54:42:43.1	lum.	0.20 ± 0.04	1.69	-	$1.02^{+0.84}_{-0.61}$	40.4	24.7
SCSO J233037.1-554338.8	23:30:32.2	-55:44:09.4	map	0.20 ± 0.04	0.99	-	$1.94^{+1.28}_{-0.83}$	78.0	73.1
SCSO J233550.6-552820.4	23:35:46.4	-55:29:21.3	lum.	0.22 ± 0.04	0.67	-	$0.03^{+0.71}_{-0.03}$	1.2	0.1
SCSO J232200.4-544459.7	23:22:01.8	-54:45:38.8	lum.	0.27 ± 0.04	1.73	-	$0.26^{+0.86}_{-0.26}$	12.0	1.7
SCSO J233522.6-553237.0	23:35:20.0	-55:32:30.9	lum.	0.29 ± 0.04	2.19	-	$0.85^{+1.60}_{-0.85}$	42.4	11.4
SCSO J233807.5-560304.9	23:38:07.7	-56:02:55.0	lum.	0.30 ± 0.04	2.60	-	< 0.64	-	-
SCSO J232956.0-560808.3	23:29:55.8	-56:08:28.2	lum.	0.32 ± 0.04	1.99	-	$2.13^{+2.75}_{-1.73}$	117.3	48.6
SCSO J232839.5-551353.8	23:28:41.0	-55:13:25.2	lum.	0.32 ± 0.05	1.00	-	$1.69^{+2.01}_{-1.32}$	92.4	32.8
SCSO J232633.6-550111.5	23:26:31.1	-55:01:26.9	lum.	0.32 ± 0.05	2.81	-	< 0.48	-	-
SCSO J233753.8-561147.6	23:37:57.1	-56:12:05.8	lum.	0.33 ± 0.04	2.94	-	$0.15^{+0.74}_{-0.15}$	8.0	0.5
SCSO J232156.4-541428.8	23:21:55.5	-54:14:20.0	lum.	0.33 ± 0.04	1.25	-	< 0.71	-	-
SCSO J233003.6-541426.7	23:30:06.3	-54:13:58.9	lum.	0.33 ± 0.04	0.88	-	$2.81^{+2.07}_{-1.47}$	159.9	75.3
SCSO J233231.4-540135.8			n/a	0.33 ± 0.04	1.67	-	-	-	-
SCSO J233430.2-543647.5			n/a	0.35 ± 0.05	3.59	-	-	-	-
SCSO J233110.6-555213.5	23:31:08.4	-55:51:38.3	lum.	0.39 ± 0.05	1.04	-	< 0.56	-	-
SCSO J233618.3-555440.3	23:32:13.8	-55:54:16.4	lum.	0.49 ± 0.03	0.94	-	$0.97^{+1.59}_{-0.97}$	77.8	8.9
SCSO J233706.3-541903.8	23:37:11.3	-54:18:57.5	lum.	0.51 ± 0.04	1.58	-	$0.85^{+3.03}_{-0.85}$	70.9	6.9
SCSO J233816.9-555331.1	23:38:12.7	-55:53:12.5	lum.	0.52 ± 0.03	1.29	-	$0.35^{+2.09}_{-0.35}$	29.1	1.5
SCSO J233556.8-560602.3	23:35:55.6	-56:05:50.5	lum.	0.52 ± 0.03	7.15	-	$1.35^{+2.03}_{-1.22}$	116.9	15.0
SCSO J232619.8-552308.8	23:26:14.5	-55:23:22.9	lum.	0.52 ± 0.03	1.25	-	$2.81^{+3.34}_{-2.22}$	249.9	52.4
SCSO J233425.6-542718.0	23:34:26.9	-54:27:32.5	lum.	0.53 ± 0.04	3.41	-	< 0.37	-	-
SCSO J232215.9-555045.6	23:22:17.0	-55:50:07.1	lum.	0.56 ± 0.04	2.40	-	$0.32^{+4.13}_{-0.32}$	28.9	1.3
SCSO J232247.6-541110.1	23:22:53.0	-54:10:54.8	lum.	0.58 ± 0.04	1.16	-	$5.11^{+5.57}_{-4.09}$	531.6	137.8
SCSO J232211.0-561847.4	23:22:13.6	-56:18:35.7	lum.	0.61 ± 0.05	5.65	-	$0.47^{+2.61}_{-0.47}$	47.6	2.3
SCSO J233731.7-560427.9	23:37:30.0	-56:04:01.2	lum.	0.61 ± 0.05	3.05	-	$2.56^{+3.87}_{-2.56}$	275.7	41.4
SCSO J234012.6-541907.2	23:40:08.8	-54:19:02.9	lum.	0.62 ± 0.04	5.23	-	< 2.56	-	-
SCSO J234004.9-544444.8	23:40:02.9	-54:44:21.0	lum.	0.66 ± 0.05	4.20	-	$6.74^{+4.45}_{-3.36}$	842.5	211.8
SCSO J232342.3-551915.1	23:23:45.5	-55:19:08.9	lum.	0.67 ± 0.04	2.72	-	< 0.51	-	-
SCSO J232829.7-544255.4	23:28:27.5	-54:42:19.3	lum.	0.68 ± 0.04	8.34	-	$0.59^{+3.12}_{-0.59}$	69.4	3.3
SCSO J233403.7-555250.7			n/a	0.71 ± 0.04	0.88	-	-	-	-
SCSO J233951.1-551331.3			n/a	0.73 ± 0.04	1.3	-	-	-	-
SCSO J233720.2-562115.1	23:37:22.4	-56:20:44.8	lum.	0.75 ± 0.03	0.70	-	$5.61^{+7.24}_{-4.87}$	835.3	151.0

NOTE. — Physical properties of SZ and optically selected clusters in the SCS regions. Redshifts represent the photometric redshift from the bright elliptical in the center of the cluster with $\pm 1\sigma$ limits. The ID is based on the position of the BCG. The NFW fit is centered at either the peak in the mass map (map) where available, or the luminosity-weighted center (lum.).